D_{4h} local symmetric dysprosium(III) single-molecule magnet with energy barrier exceeding 2000 K

Xia-Li Ding [a], Yuan-Qi Zhai [a], Tian Han [a]*, Wei-Peng Chen [a], You-Song Ding [a] and Yan-Zhen Zheng [a]*

Three six-coordinate Dy(III) single-molecule magnets (SMMs) $[Dy(O^tBu)_2(L)_4]^+$ with D_{4h} local symmetry are obtained by optimising the equatorial ligands. Compound 1 where L = 4-phenylpyridine shows an energy barrier (U_{eff}) of 2075(11) K, which is the third largest U_{eff}, and the first U_{eff} > 2000 K for SMMs with axial-type symmetry so far.

With progressive advances in enhancing energy barriers for magnetization reversal (U_{eff}) and blocking temperatures (T_B) of single-molecule magnets (SMMs), only two dysprosium(III) metallocenium complexes $[(Cp^{ipr5})Dy(Cp^*)][B(C_6F_5)_4]$ and $[(Cp^{ipr5})Dy(Cp^{ipr4Me})][B(C_6F_5)_4]$ have U_{eff} over 2000 K up to date.[1,2] Since the intrinsic magnetisms of SMMs are closely related to the structures of compounds, the critical target is to explore efficient means and chemically feasible routes to increase the U_{eff} and T_B,[3] so that SMMs can be applied in practice.[4] Theoretical and experimental studies have shown that the magnetic dynamics of lanthanide SMMs can be tailored by the coordination geometries and ligand fields around the metal centers.[3,5] Thus controlling the coordination numbers in lanthanide complexes, especially in Dy(III) complexes seem to be quite attractive for better molecular magnets.[6,7] In fact, some high local-symmetry Dy(III) complexes are justified to possess large magnetic anisotropies and to exhibit significantly high U_{eff}.[1,2,8-11] For example, Dy(III) ions in recent SMMs often situate in a D_{5h} local symmetry, where the axial anisotropies are defined by the strong coordination bonds along the C_5 axis.[10] Meanwhile, Murrie and our two groups reported series of eight-coordinate Dy-based SMMs with D_{6h} local symmetries showing U_{eff} over 1000 K.[11]

According to the crystal field theory the majority of the non-axial crystal field terms ($\boldsymbol{B_k^q}$, q ≠ 0) can be excluded in the ideal D_{4h} local symmetry, since the Hamiltonian in it reads $\boldsymbol{H_{CF}} = \boldsymbol{B_2^0\bar{O}_2^0 + B_4^0\bar{O}_4^0 + B_4^4(\bar{O}_4^4 + \bar{O}_4^{-4}) + B_6^0\bar{O}_6^0}$, and only the non-axial crystal field term $\boldsymbol{B_4^4}$ can be retained.[12-14] Therefore, in such circumstance both U_{eff} and T_B may be increased, probably improving the properties of the SMMs with D_{4h} local symmetry. However, six-coordinate Dy(III) complexes are scarce and only some have been reported as mononuclear SMMs until now, let alone the six-coordinate mononuclear Dy SMMs with D_{4h} symmetry (Table S1).[15] Unfortunately, the U_{eff} for the six-coordinate mononuclear Dy(III) SMMs are below 1100 K, and most show poor U_{eff}. Their local coordination geometries are mostly pseudo-octahedrons (denoted by O_h), -trigonal prisms (D_{3h}) or -anti trigonal prisms (D_{3d}), and only two compressed octahedrons (D_{4h}). One distorted D_{4h} local symmetric SMM is $[Dy(DiMeQ)_2Cl_3(H_2O)]$ with the high U_{eff} of 1100 K which benefits from short Dy-O bonds,[15a] and the other is $[DyR_2(py)_4][BPh_4]\cdot 2py$ (R = carbazolyl) with U_{eff} of 70 K.[15b]

In view of the situation above, we decided to construct mononuclear Dy(III) complexes with D_{4h} symmetry while maintaining strong coordination bonds along axial direction based on our previously developed D_{5h} method.[10c] We chose some sterically bulky pyridine derivatives (L) as equatorial ligands and set tert-butoxide ($^-O^tBu$) ligands in the axial positions (Scheme S1). Three complexes $[Dy(O^tBu)_2(L)_4]^+$ with D_{4h} local symmetry, where L = 4-phenylpyridine (**1**); L = 1-4-piperidin-1-ylpyridine (**2**); L = 4-pyrrolidin-1-ylpyridine (**3**) were successfully synthesized. Magnetic studies show that they feature high U_{eff} of 2075(11), 1886(9) and 1810(5) K for **1**, **2** and **3**, respectively. This not only achieves the third largest U_{eff}, and the first one over 2000 K with axial symmetry in SMMs until now, but also offers a unique design strategy towards a class of Dy-based hexa-coordinate complexes with D_{4h} local symmetry.

Single crystal X-ray diffraction shows that **1** crystallizes in the cubic space group *Pn*-3n, while **2** and **3** crystallize in the triclinic space group *P*-1 (Table S2). Complex **2** comprises of two six-coordinate Dy(III) cations $[Dy(O^tBu)_2(L)_4]^+$ (Fig. 1a) and two charge-balancing anions BPh_4^- in the crystallographic asymmetric unit, while **1** and **3** differ in having inversion centers/axial symmetries at Dy(III) sites in the asymmetric unit. The structures for **1**-**3** all contain $[Dy(O^tBu)_2(L)_4]^+$ motif with one Dy^{3+} ion in the center, two axial $^-O^tBu$ ligands in the trans positions and four neutral 4-pyridine derivative ligands at the equatorial plane. The $^-O^tBu$ anions are very basic, leading to short Dy–O bond lengths of 2.070(7) Å for **1**, 2.121(5) and 2.112(4) Å (for Dy1) as well 2.122(5) and 2.149(5) Å (for Dy2) in **2**, 2.133(5) Å (for Dy1) and 2.141(5) Å (for Dy2) in **3** (Table S3). The four equatorial Dy–N bond lengths average at 2.471(6) Å for **1**, 2.511(6) Å for **2**, and 2.512(6) Å for **3**, much longer than that of Dy–O bonds. The axial O–Dy–O angles are 180.0, 178.80(15) and 180.0(3)° for **1**, **2** and **3**, respectively, showing an essentially linear coordination between Dy and O atoms. Meanwhile, four equatorial N–Dy–N angles range from 90.0 (1) to 90.0(3)° for **1**, 85.39(16)–95.79(17)° for **2** and 86.54(15)–93.55(17)° for **3**, from which we can see **1** possesses the closest right angle of 90°. Nevertheless, the coordination polyhedra of the Dy(III) ions in these three complexes are all pseudoctahedral with axially compressed feature (Fig. 1b). We also used the SHAPE 2.0 program to measure the geometric

[a] *Frontier Institute of Science and Technology (FIST), School of Chemistry, Xi'an Jiaotong University Shenzhen Research School, State Key Laboratory for Mechanical Behavior of Materials, MOE Key Laboratory for Nonequilibrium Synthesis and Modulation of Condensed Matter, Xi'an Jiaotong University, Xi'an 710049, China*

E-mail: hantian0123@xjtu.edu.cn; zheng.yanzhen@xjtu.edu.cn

Electronic Supplementary Information (ESI) available: Synthetic procedures, structures, crystallographic details and additional figures. CCDC 1970693 (**1**), 1970684 (**2**) and 1970683 (**3**). For ESI and crystallographic data in CIF or other electronic format. See DOI: 00.0000/0000000000

distortion degree from ideal octahedron [16], which shows only slight deviations from O_h to D_{4h} symmetry due to the compressed axial bonds of the DyO_2N_4 coordination sphere (Table S4). The shortest intermolecular Dy···Dy distances are 15.64(3), 14.69(4) and 12.14(5) Å for **1**, **2** and **3**, respectively (Figs. S4–S6).

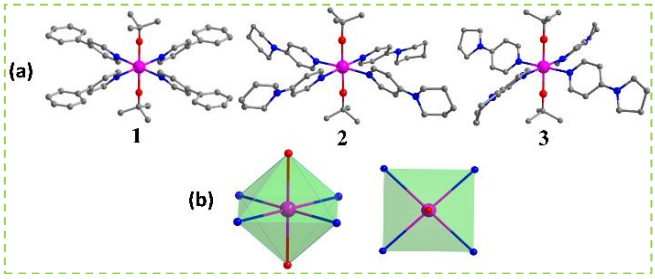

Fig. 1 Crystal structures of the $[Dy(O^tBu)_2(L)_4]^+$ cations in **1**-**3** (a). Color code: Dy (pink), N (blue), O (red) and C (gray). Other atoms are omitted for clarify. The coordination polyhedrons of the Dy(III) ions for **1**-**3** seen from front and from top to bottom (b). The formulae are determined as $Na\{[Dy(O^tBu)_2(4\text{-}Phpy)_4][BPh_4]\}\cdot 2THF\cdot hex$ for **1**, $[Dy(O^tBu)_2(4\text{-}Pdpy)_4][BPh_4]$ for **2** and $[Dy(O^tBu)_2(4\text{-}Plpy)_4][BPh_4]$ for **3**.

The temperature dependence of magnetic susceptibility was carried out under 1000 Oe dc field in the temperature range of 2–300 K. At 300 K, the χT products are 14.01, 14.06 and 14.09 $cm^3\ K\ mol^{-1}$ for **1**, **2** and **3**, respectively, close to the expected value of 14.17 $cm^3\ K\ mol^{-1}$ for one free Dy(III) ion ($^6H_{15/2}$). Upon cooling, χT values keep almost constant with a slight decrease above about 20 K. Further cooling gives a sudden drop of the χT values to 8.75, 7.36 and 6.14 $cm^3\ K\ mol^{-1}$ at 2 K for **1**, **2** and **3**, respectively (Fig. S7). The field (H) dependence of the magnetization (M) increases slowly to the maximum values of 5.01, 5.04 and 5.03 μ_B for **1**, **2** and **3** at 2 K, respectively (Fig. S7, insert). Zero-field-cooled and field-cooled (ZFC-FC) magnetizations show divergence at 5 K for **1**, a ZFC-peak at 4 K for **2** and 5 K for **3** (Fig. S8). Applying a scanning rate of 1 mT s^{-1}, butterfly-like loops can be observed and remain open up to 5 K for **1**, 8 K for **2** and **3** (Fig. S9). When scanning rate of 20 mT s^{-1} is applied for **1**, the magnetic hysteresis loops are not fully closed up to 25 K (Fig. S9d).

Significant temperature-dependence and frequency-dependence in alternating current (ac) susceptibilities under zero dc field can be observed up to 118 K for **1**, 100 K for **2** and **3** at 1218 Hz (Figs. S10 and S11). The in-phase (χ') and out-of-phase (χ'') components show one relaxation process for **1**-**3**, and thus we fit the Cole–Cole plots with a modified Debye function (Figs. S12–S14). All the α values are less than 0.1 (T > 20 K), indicating a narrow distribution of relaxation times. However, α become substantially larger at lower temperatures due to the onset of a different relaxation mechanism (Tables S5–S7). As shown in the plots of τ^{-1} vs. T (Fig. 2), the τ^{-1} value increases smoothly as the temperature rises in the low temperature region while rapidly in the high temperature region, indicative of the presence of two magnetic relaxation mechanisms for **1**-**3**. The τ values are then fitted with the equation $\tau^{-1} = \tau_0^{-1}e^{-U_{eff}/T} + CT^n$, giving the following parameters: for **1**, U_{eff} = 2075(11) K, τ_0 = 5.61(2)×10^{-13} s, C = 5.60(4)×10^{-3} $s^{-1}\ K^{-n}$, n = 2.93(4); for **2**, U_{eff} = 1886(9) K, τ_0 = 1.36(4)×10^{-12} s, C = 1.49(3)×10^{-3} $s^{-1}\ K^{-n}$, n = 2.90(3); for **3**, U_{eff} = 1810(5) K, τ_0 = 2.13(5)×10^{-12} s, C = 1.94(2)×10^{-3} $s^{-1}\ K^{-n}$, n = 3.02(5). This result suggests that the intrinsic relaxation mechanisms are similar in three complexes, namely the dominated Orbach relaxation mechanism in high temperature region and Raman relaxation mechanism in low temperature. It also shows that the relaxation times in Orbach region for **2** and **3** are always shorter than that of **1** at the same temperature, and this is probably the reason why the U_{eff} for **1** is larger.

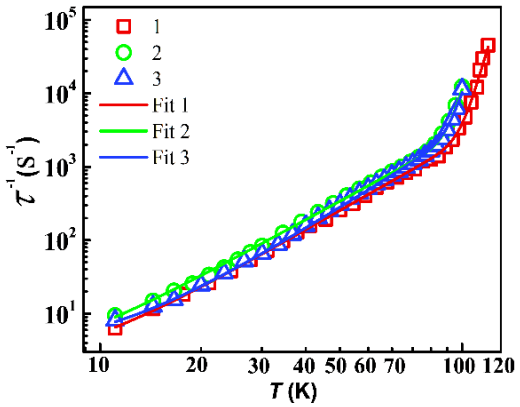

Fig. 2 Temperature dependence of the relaxation time τ in zero dc field for **1** (red), **2** (green) and **3** (blue). The solid lines are the best fits.

To reveal the mechanism that governs the magnetic relaxation, we have performed *ab-initio* calculations using the CASSCF/RASSISO/SINGLE–ANISO approach implemented in MOLCAS 8.2 (see Supporting Information for details).[17] The eight Kramers Doublets (KDs), corresponding to the $^6H_{15/2}$ state of Dy(III) ion, span an energy barrier of ~2400 K for **1**–**3** (Tables S10–S12). The ground state (m_J = $|\pm 15/2>$) is highly anisotropic (g_z = 19.98 for **1**, 19.88 for **2** and 19.89 for **3**) with negligible transverse components. The main magnetic anisotropy axis is nearly collinear with the *pseudo*-C_4 axis lying along the axial O-Dy-O orientation (Figs. 3 insert, S18 and S20). This can also be explained with the LoProp[18] charges computed using the CASSCF wave functions (Table S13, Figs. S22–24). The charge on the axial O atoms is found to be nearly three times larger than the N atoms of pyridine derivative.

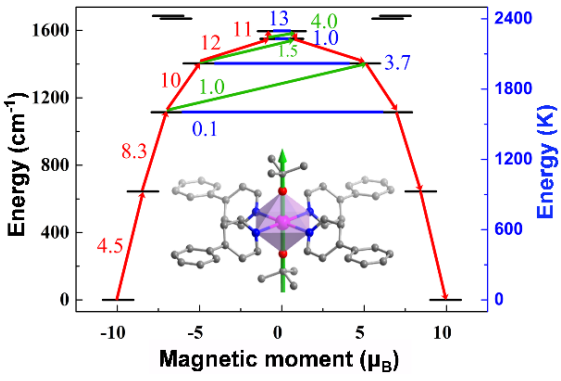

Fig. 3 Ab initio calculated electronic states of the J = 15/2 manifold of the $^6H_{15/2}$ term of Dy(III) in **1**. The principal magnetic axis of the ground Kramer's doublet of 1 (insert). The connected energy states with the number representing matrix element of the transverse moment are shown by the arrows. The KDs as function of magnetic moments are illustrated by the black line. The blue solid arrow indicates the QTM via ground state and TA-QTM (thermally assisted QTM) via excited states. The green solid arrow presents possible Orbach relaxation mechanism. The mechanism of magnetic relaxation is indicated by the red arrow.

The two excited states m_J = |±13/2> (KD_2) and m_J = | ±11/2> (KD_3) are also axial in nature (Tables S10–S12), and lie at 926 and 1601 K for **1**, 870 and 1497 K for **2** and 828 and 1418 K for **3** above the ground state. The relatively larger g_x/g_y values obtained for the next excited state (KD_4) with m_J = 83%|±9/2> + 10%|±1/2>, g_x = 2.25, g_y = 2.37, g_z = 11.02 for **1**; m_J = 76%|±9/2> + 12%|±1/2>, g_x = 3.32, g_y = 3.49, g_z = 10.08 for **2** and m_J = 77%|±9/2> + 20%|±1/2>, g_x = 4.43, g_y = 4.71, g_z = 9.12 for **3**, yield larger magnetic moment matrix elements of 3.7 μ_B^2 for **1**, 4.7 μ_B^2 for **2** and 3.6 μ_B^2 for **3**, which are sufficient to promote magnetic relaxation via this state. The subsequent excited states are highly mixed and bunched over 2228~2424 K for **1**; 2052~2222 K for **2** and 1911~2070 K for **3**. We predict the most efficient magnetic relaxation pathway to occur is via the highly bunched set of states with calculated magnetization reversal barriers (Δ_E) of 2018~2293 K, 1869~2052 K and 1751~1911 K for **1**, **2** and **3**, respectively (Fig. 3, S19, S21) Hence, the calculated and experimental magnetization reversal barriers are in close agreement.

Crystal field parameters (CFPs) defined by the full sets of Hamiltonian $H_{CF} = \sum_{k=2,4,6}\sum_{q=-k}^{k} B_k^q \tilde{O}_k^q$ are calculated by using the SINGLE_ANISO program (Tables S14–S16). Firstly, the parameter B_4^4 for each compound (-0.060 for **1**, -0.036 for **2** and -0.034 for **3**) is equal in magnitude to the axial parameter B_4^0 (-0.014 for **1**-**3**), accounting for their sharp decrease of magnetization under zero field in hysteresis loops (Fig. S9). Besides transverse CFPs, the sharp drop on zero field could be also caused by magnetic dipolar interactions or hyperfine interaction. Secondly, the axial parameter B_2^0 which takes main responsibility for the axiality of ground KDs is further studied. The result shows that B_2^0 are negative for all compounds, with the biggest value for **1** (-9.50 for **1**, -8.61 for **2** and -7.91 for **3**), suggesting strong uniaxial anisotropies for **1**–**3** (Tables S14-S16). Meanwhile, the other axial terms (B_4^0 and B_6^0) are similar to each other for **1**-**3**. For the terms with ranking k = 2, the transverse ones (B_k^q, q $\neq$ 0) are at least one order of magnitude smaller than the axial terms (B_k^q, q = 0). However, for those with k = 4, the transverse parameters B_4^4 are larger than the axial terms while others are comparable or smaller. Besides, for those with ranking k = 6, all terms are of the same magnitude. We conclude that the presence of these transverse terms of B_k^q (q ≠ 0) is due to some but slight distortions from ideal symmetry in real geometry of **1**–**3** (Table S4) as mentioned before. However, since non-axial crystal field terms in low-ranking ones, namely B_k^q, q ≠ 0, k = 2, 4, except for B_4^4, are relatively small, while the low-ranking terms have greater contribution than the high-ranking ones (k = 6), complexes **1**–**3** can be predicted to possess nearly perfect tetragonal bipyramid local symmetries. In sum, the local symmetry of D_{4h} with a compressed electrostatic potential in axial direction can lead to a strong magnetic anisotropy and partially suppressed QTM effect. Moreover, the more charge the two coordinated O atoms carry, the shorter the average Dy-O bond length and the higher the energy barrier will be. This suggests that the D_{4h} geometry is a viable one for the design of new class of SMMs.

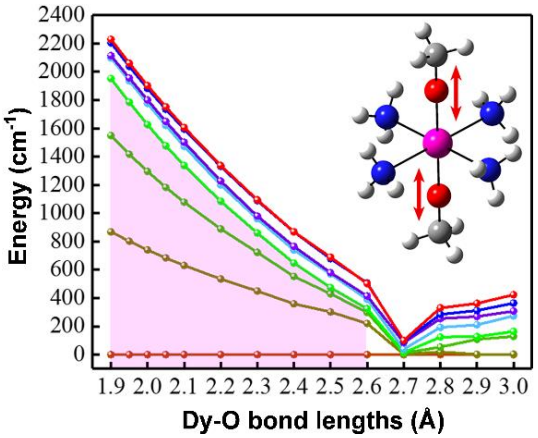

Fig. 4 Evolution of the energy spectrum of eight Kramers doublets upon elongation and contraction of two axial Dy–O chemical bonds. The highlighted region defines the most possible blocking barrier; Structure of the model complex $[Dy(OMe)_2(NH_3)_4]^+$ (insert).

To further exemplify this effect, we investigate a model complex $[Dy(OMe)_2(NH_3)_4]^+$ with exact D_{4h} local symmetry but different Dy–O bond lengths (Fig. 4, inset). In this model, the $^-O^tBu$ is simplified into ^-OMe at axial positions with linear O-Dy-O angle, and the four equatorial pyridine ligands are replaced by NH_3 molecules while the nearest ∠N-Dy-N are fixed to 90°. The Dy–O bond lengths are varied from 1.9 to 3.0 Å in order to study the effect of compression along the axis (Fig. 4). The calculated *g* tensor of the ground doublet state in this octahedral $[Dy(OMe)_2(NH_3)_4]^+$ complex is highly anisotropic with a pure ground-state m_J = ±15/2 multiplet of Dy^{3+} and $g_x = g_y \approx 0$, $g_z \approx 20$ when Dy–O bond lengths range from 1.9 to 2.6 Å (Table S20). In this region, the energies of all seven excited KD states increase linearly upon large contraction of Dy–O bond lengths. Specifically, the most possible blocking barriers of the deformed structures shown by the highlighted region in Fig. 4 are lifted significantly by the contraction. When the Dy–O bond is elongated to 2.7 Å, the ground KD *g* tensor becomes isotropic with $g_x \approx g_y \approx g_x \approx 6$. Thus, the crystal field splitting of excited KDs drops sharply as the Dy–O bond length increases from 2.6 to 2.7 Å. Further elongation leads to the easy-plane type magnetic anisotropy in the ground state. These ground states are then no longer m_J = ±15/2 multiplet but m_J = ±1/2, and no energy barrier can be predicted for these deformed structures.

In summary, by combining strong uniaxial crystal field with weak transverse crystal field, we obtained three mononuclear six-coordinate Dy(III) SMMs $[Dy(O^tBu)_2(L)_4]^+$ with D_{4h} local symmetry. Magnetic studies and *ab initio* analysis corroborate that **1** has a record U_{eff} of 2075(11) K for axially symmetric SMMs. Further fine-tuning the bond lengths of axial ligands through the theoretical model gives the compression ratio of the octahedral geometry which is direct in proportion to the U_{eff}. Such a high performance of Dy-SMMs with D_{4h} local symmetry presents a new way to construct excellent SMMs. Future work would include improving rigidity of complexes to reduce the Raman process.

This work was supported by NSFC (21871219 and 21773130), Key Laboratory Construction Program of Xi'an Municipal Bureau of Science and Technology (201805056ZD7CG40), China Postdoctoral Science Foundation (2019T120891 and

2018M631138), Key Scientific and Technological Innovation Team of Shaanxi province (2020TD-001), Shenzhen Science and Technology Program (JCYJ20180306170859634), and Fundamental Research Funds for the Central Universities. We thank the Instrument Analysis Center of Xi'an Jiaotong University for the assistance from Dr. Gang Chang.

Conflicts of interest

The authors declare that they have no conflict of interest.

Notes and references

1 F.-S. Guo, B. M. Day, Y. C. Chen, M.-L. Tong, R. A. Layfield, *Science*., 2018, **362**, 1400.
2 K. R. McClain, C. A. Gould, K. Chakarawet, S. J. Teat, T. J. Groshens, J. R. Long, B. G. Harvey, *Chem. Sci.,* 2018, 8492.
3 (a) M. J. Giansiracusa, A. K. Kostopoulos, D. Collison, R. E. P. Winpenny, N. F. Chilton, *Chem. Commun*., 2019, **55**, 7025; (b) Z. Zhu, M. Guo, X.-L. Li, J. Tang, *Coord. Chem. Rev.,* 2019, **378**, 350; (c) J.-L. Liu, Y.-C. Chen, M.-L. Tong. *Chem Soc Rev.,* 2018, **47**, 2431; (d) F. Pointillart, O. Cador, B. Le Guennic, L. Ouahab, *Coord. Chem. Rev*., 2017, **346**, 150; (e) S. GómezCoca, D. Aravena, R. Morales, E. Ruiz, *Coord. Chem. Rev.,* 2015, **289**, 379.
4 (a) M. N. Leuenberger and D. Loss, *Nature*, 2001, **410**, 789; (b) M. Urdampilleta, S. Klyatskaya, J.-P. Cleuziou, M. Ruben and W. Wernsdorfer, *Nat. Mater.*, 2011, **10**, 502; (c) S. Thiele, F. Balestro, R. Ballou, S. Klyatskaya, M. Ruben and W. Wernsdorfer, *Science*, 2014, **344**, 1135.
5 (a) J. D. Rinehart, J. R. Long, *Chem. Sci.* 2011, **2**, 2078; (b) L Ungur, L F Chibotaru, *Phys Chem Chem Phys*., 2011, **13**, 20086; (c) N. F. Chilton, C. A. P. Goodwin, D. P. Mills, R. E. P. Winpenny, *Chem. Commun*., 2015, **51**, 101.
6 (a) N. Ishikawa, M. Sugita, T. Ishikawa, S.-Y. Koshihara, Y. Kaizu, *J. Am. Chem. Soc*., 2003, **125**, 8694. (b) C. R. Ganivet, B. Ballesteros, G. de la Torre, J. M. Clemente-Juan, E. Coronado, T. Torres, *Chem. Eur. J.*, 2013, **19**, 1457 (c) P. Zhang, L. Zhang, C. Wang, S. Xue, S.-Y. Lin, J. Tang, *J. Am. Chem. Soc*., 2014, **136**, 4484; (d) S. M. Chen, J. Xiong, Y. Q. Zhang, Q. Yuan, B. W. Wang, S. Gao, *Chem. Sci.,* 2018, **9**, 7540; (e) K. L. M. Harriman, J. L. Brosmer, L. Ungur, P. L. Diaconescu, M. Murugesu, *J. Am. Chem. Soc.*, 2017, **139**, 1420; (f) Y. S. Meng, L. Xu, J. Xiong, Q. Yuan, T. Liu, B. W. Wang, S. Gao, *Angew. Chem. Int. Ed*., 2018, **57**, 4673; (g) P.-B. Jin, Y.-Q. Zhai, K.-X. Yu, R. E. P. Winpenny, Y.-Z. Zheng, *Angew. Chem*. *Int. Ed*., 2020, 59, 9350.
7 N. F. Chilton, *Inorg. Chem*., 2015, **54**, 2097.
8 (a) C. A. P. Goodwin, F. Ortu, D. Reta, N. F. Chilton, D. P. Mills, *Nature*, 2017, **548**, 439. (b) S. K. Gupta, T. Rajeshkumar, G. Rajaraman, R. Murugavel, *Chem. Sci.*, 2016, **7**, 5181.
9 (a) Y. S. Meng, L. Xu, J. Xiong, Q. Yuan, T. Liu, B. W. Wang, S. Gao*, Angew. Chem. Int. Ed.,* 2018*,* **130***, 4763*; (b) Y.-S. Ding, K.-X. Yu, D. Reta, F. Ortu, R. E. P. Winpenny, Y.-Z. Zheng, N. F. Chilton, *Nat. Commun*., 2018, **9**, 3134.
10 (a) J. L. Liu, Y. C. Chen, Y. Z. Zheng, W. Q. Lin, L. Ungur, W. Wernsdorfer, L. F. Chibotaru, M. L. Tong, *Chem. Sci*., 2013, **4**, 3310; (b) Y.-C. Chen, J.-L. Liu, L. Ungur, J. Liu, Q.-W. Li, L.-F. Wang, L. F. Chibotaru, X.-M. Chen, M.-L. Tong, *J. Am. Chem. Soc*., 2016, **138**, 2829; (c) Y.-S. Ding, N. F. Chilton, R. E. P. Winpenny, Y.-Z. Zheng, *Angew. Chem. Int. Ed*., 2016, **55**, 16071; (d) A. B. Canaj, M. K. Singh, C. Wilson, G. Rajaraman, M. Murrie, *Chem. Commun*., 2018, **54**, 8273; (e) Y.-S. Ding, T. Han, Y.-Q. Zhai, N. F. Chilton, R. E. P. Winpenny, Y.-Z. Zheng, *Chem. Eur. J.,* 2020, 26, 5893.
11 (a) A. B. Canaj, Sourav Dey, E. R. Marti, Claire Wilson, Gopalan Rajaraman, Mark Murrie, *Angew. Chem. Int. Ed*., 2019, **131**, 14284; (b) Z.-H. Li, Y.-Q. Zhai, W.-P. Chen, Y.-S. Ding, and Y.-Z. Zheng, *Chem. Eur. J*., 2019, **25**, 16219.
12 (a) L. Ungur, L. F. Chibotaru, *Inorg. Chem*., 2016, **55**, 10043; (b) M.-J. Liu, J. Yuan, Y.-Q. Zhang, H.-L. Sun, C.-M. Liu, H.-Z. Kou, *Dalton Trans*., 2017, **46**, 13035; (c) E. M. Pineda, C. Godfrin, F. Balestro, W. Wernsdorfer, M. Ruben, *Chem. Soc. Rev.,* 2018, **47**, 501.
13 (a) M. Gregson, N. F. Chilton, I. F. Crowe, W. Lewis, A. J. Blake, D. Collison, R. E. P Winpenny, S. T. Liddle, *Chem. Sci*., 2016, **7**, 155; (b) R. J. Blagg, L. Ungur, F. Tuna, J. Speak, P. Comar, D. Collison, W. Wernsdorfer, E. J. McInnes, L. F. Chibotaru, R. E. P Winpenny, *Nat. Chem*., 2013, **5**, 673.
14 (a) J. Liu, Y.-C. Chen, J.-H. Jia, J.-L. Liu, V. Vieru, L. Ungur, L. F. Chibotaru, Y. Lan, W. Wernsdorfer, S. Gao, X.-M. Chen, M.-L. Tong, *J. Am. Chem. Soc.,* 2016, **138**, 5441; (b) A. K. Bar, C. Pichon, J. P. Sutter, *Coord. Chem. Rev*., 2016, **308**, 346.
15 Only some literatures of six-coordinate mononuclear Dy(III) SMMs are listed, for more information please see SI. (a) J. G. Marcus, A. B. Susan, K. K. Andreas, F. S. George, D. C. Whitehead, Floriana Tuna, R. E. Winpenny, F. C. Nicholas, *Dalton Trans*., 2019, **48**, 10795; (b) J. Long, A. N. Selikhov, E. Mamontova, K. A. Lyssenko, Y. Guari, J. Larionova, A. Trifonov*, Dalton Trans.*, 2020, 49, 4039.
16 D. Casanova, J. Cirera, M. Llunell, P. Alemany, D. Avnir and S. Alvarez, *J. Am. Chem. Soc*., 2004, **126**, 1755.
17 (a) F. Aquilante, J. Autschbach, R. K. Carlson, L. F. Chibotaru, M. G. Delcey, L. De Vico, I. Fdez Galvan, N. Ferre, L. M. Frutos, L. Gagliardi, et al., *J. Comput. Chem.,* 2016, **37**, 506; b) L. F. Chibotaru, L. Ungur, *J. Chem. Phys.,* 2012, **137**, 064112; c) A. A. Granovsky, *J. Chem. Phys*., 2011, **134**, 214113.
18 L. Gagliardi, R. Lindh, G. Karlstrom, *J. Chem. Phys.,* 2004, **121**, 449.